Electronic Supplementary Material (ESI) for Journal of Materials Chemistry A.

Supplementary Figures:

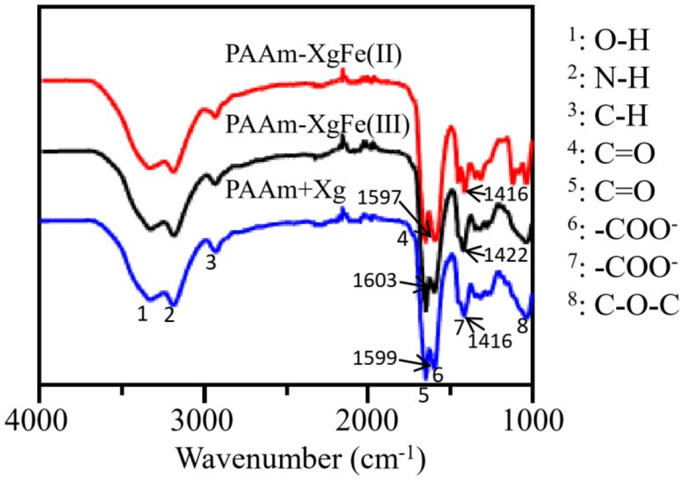

Figure S1. The FTIR spectra. The functional groups corresponding to the infrared absorption peaks were listed beside the figure. Of note, the asymmetric and symmetric stretching vibrations of COO^- groups were separately located at 1599 cm^{-1} and 1416 cm^{-1} for the PAAm+Xg (3% w/v) hydrogel, at 1603 cm^{-1} and 1422 cm^{-1} for the PAAm-XgFe(III)-3 hydrogel, and at 1597 cm^{-1} and 1416 cm^{-1} for the PAAm-XgFe(II)-3 hydrogel.

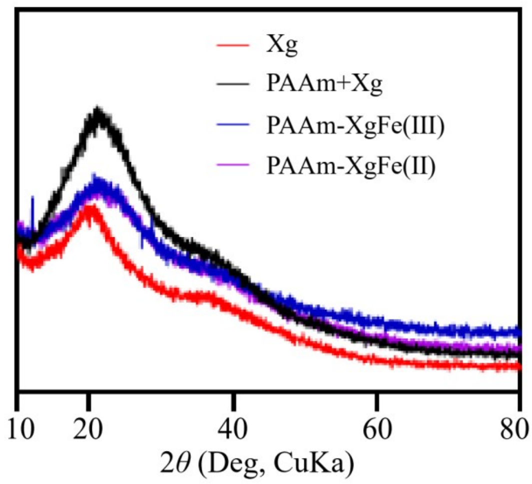

Figure S2. The XRD measurement. The peaks at around 20° were decreased in the PAAm-XgFe(III)-3 hydrogel and the PAAm-XgFe(II)-3 hydrogel compared with that in the PAAm+Xg (3% w/v) hydrogel. The peaks at around 38° represented the amorphous structure of xanthan gum.

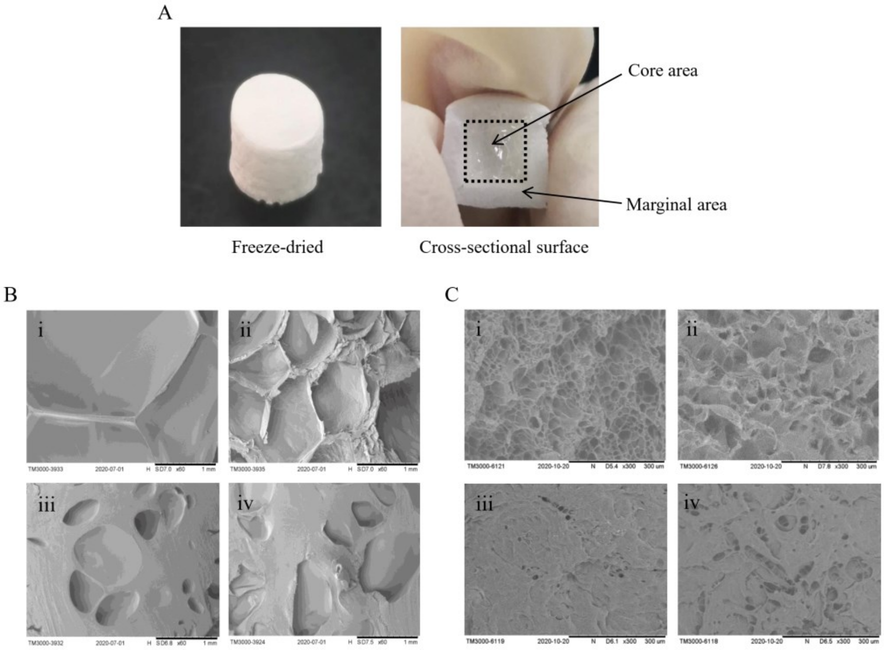

Figure S3. The morphology of PAAm-based hydrogels. (A) The general view of the freeze-dried PAAm hydrogel and its cross-sectional surface with a clear border dividing the core and marginal areas. (B) The SEM morphology at the core area of hydrogels. (C) The SEM morphology at the marginal area of hydrogels. (i): PAAm hydrogel; (ii): PAAm+Xg (3% w/v) hydrogel; (iii): the PAAm+XgFe(III)-3 hydrogel; and (iv): the PAAm+XgFe(II)-3 hydrogel.

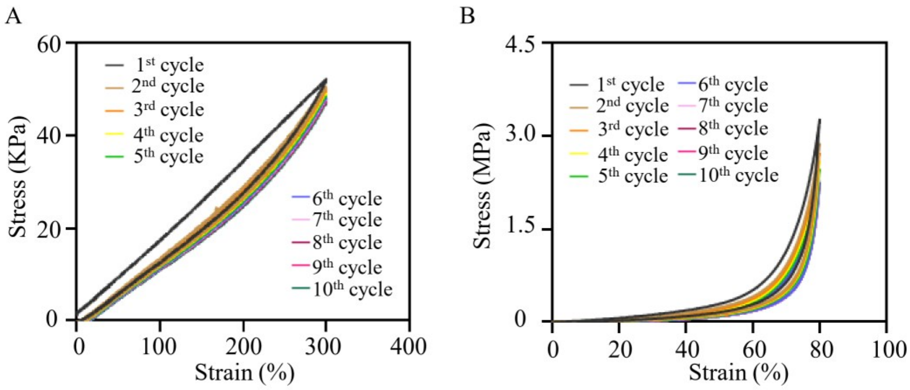

Figure S4. A ten-cycle stretch-recovery measurement of the PAAm-XgFe(II)-3 hydrogel (A), and a ten-cycle compression-recovery test of the PAAm-XgFe(II)-3 hydrogel (B).

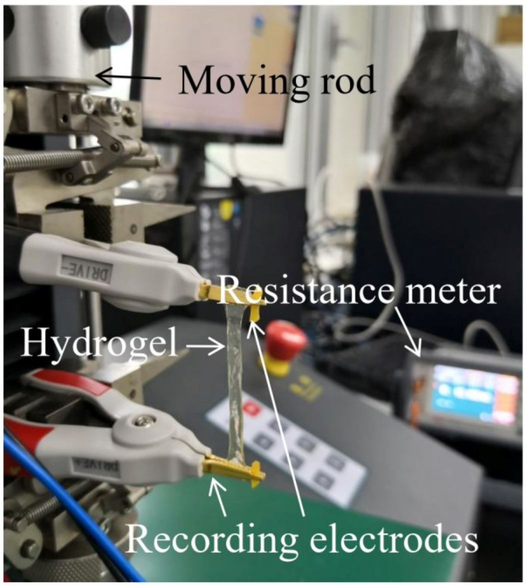

Figure S5. The machine assembled from an automatic resistance meter with a MTS for the detection of the electromechanical properties.

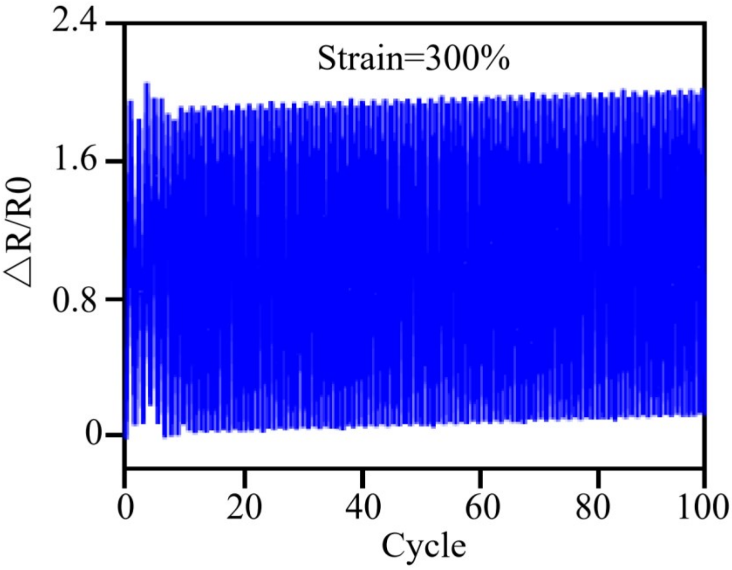

Figure S6. The measurement of the relative resistance change for 100 stretch-recovery cycles in the range of 0%–300% strain.

PAAm+Xg hydrogel PAAm-XgFe(III) hydrogel PAAm-XgFe(II) hydrogel

Figure S7. The light transmittance of the university badge covered with the PAAm+Xg (3% w/v) hydrogel, the PAAm-XgFe(III)-3 hydrogel, or the PAAm-XgFe(II)-3 hydrogel.

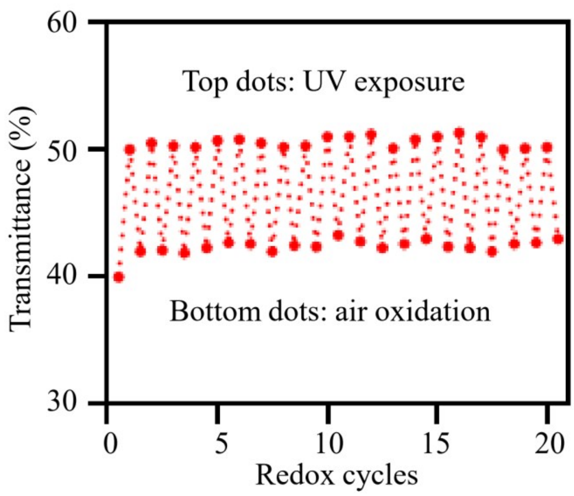

Figure S8. The light transmittance of hydrogels during the twenty cycles of the Fe(III)/Fe(II) redox.

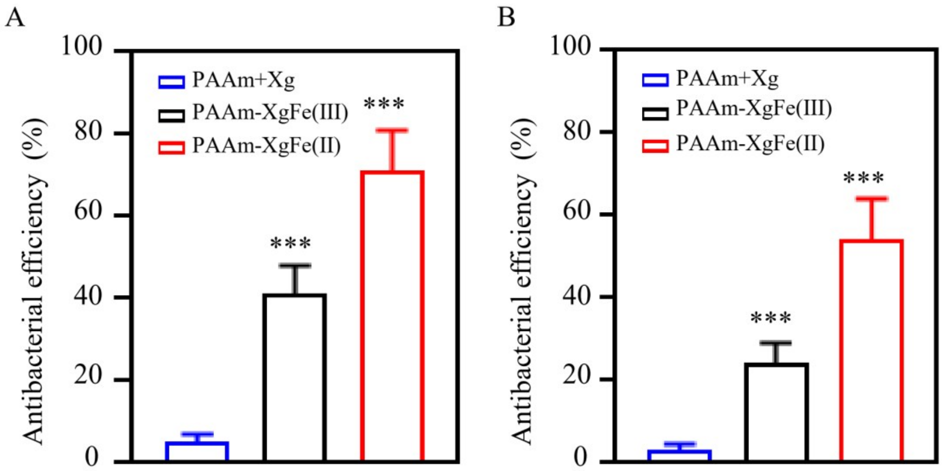

Figure S9. The antibacterial efficiency against *E. coli* (A) and *S. aureus* (B) was quantified from the ratio of the red staining bacteria to the total of the bacteria. ***, P<0.001, compared with the PAAm+Xg (3% w/v) hydrogel using the Student's *t* test.

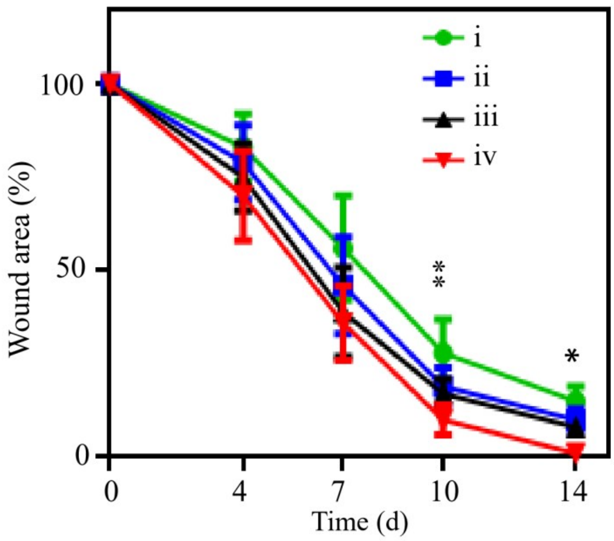

Figure S10. The percentage of wound area treated with the normal saline (i), the PAAm+Xg (3% w/v) hydrogel (ii), the PAAm-XgFe(III)-3 hydrogel (iii), and the PAAm-XgFe(II)-3 hydrogel (iv). *, P<0.05; **, P<0.01, one-way ANOVA was used for data analysis.

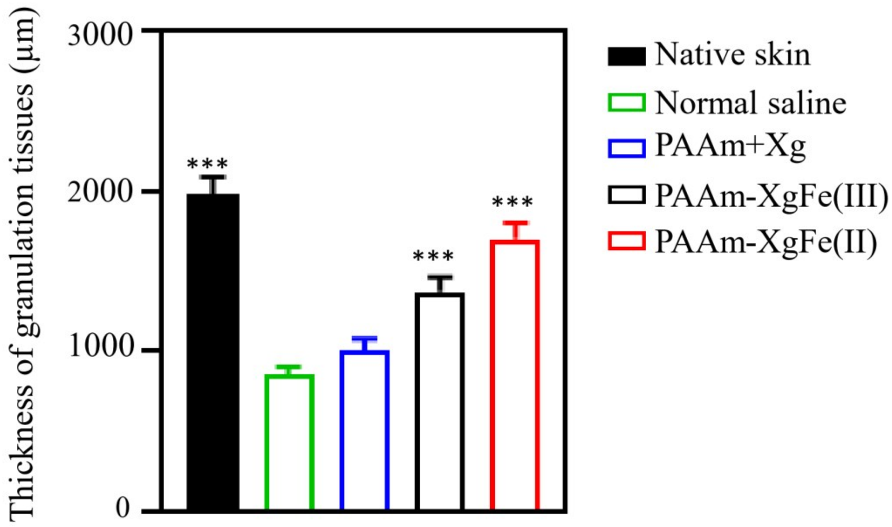

Figure S11. The thickness of the regenerated tissues on the 4th day. ***, P<0.001, compared with the infected wounds treated with normal saline using the Student's *t* test.

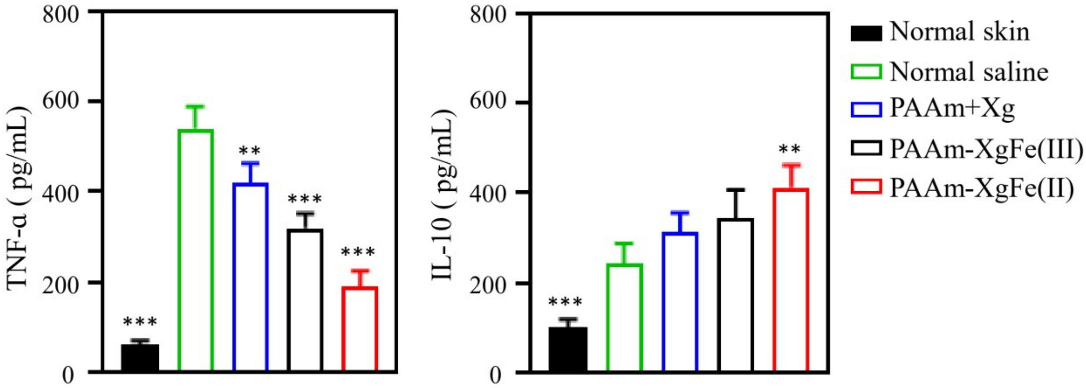

Figure S12. The expression of pro-inflammatory cytokines (TNF-α) and anti-inflammatory cytokines (IL-10) in the regenerated tissues on the 4th day. **, p<0.01; ***, P<0.001, compared with the infected wounds treated with normal saline using the Student's *t* test.

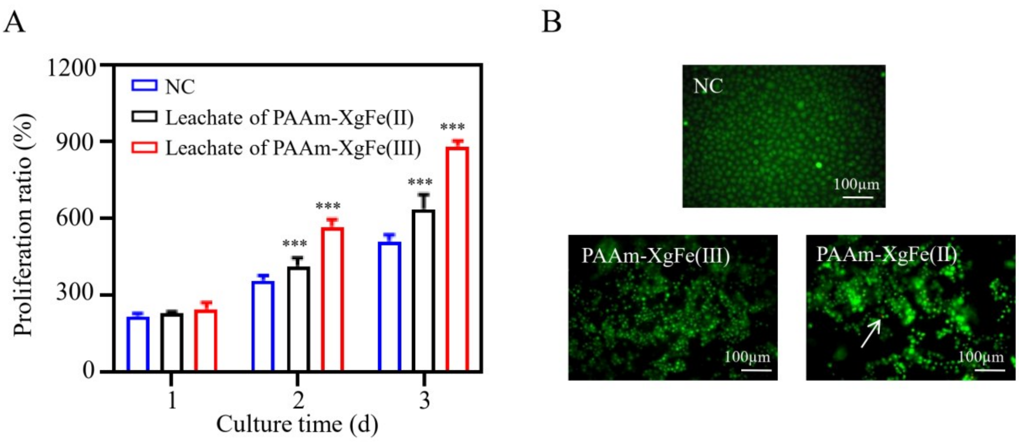

Figure S13. The biocompatible studies. (A) The proliferation of L929 fibroblasts in the different DMEM media-extracted hydrogel leachates. ***, $P<0.001$, compared with the normal culture media using the Student's *t* test. (B) The live/dead assay of L929 fibroblasts cultured on the hydrogel surface at day 3, which showed the good cytocompatibility of PAAm-XgFe(III) and PAAm-XgFe(II). While arrow: very few dead cells labeled in red.